International Journal of Microwave and Wireless Technologies

cambridge.org/mrf

Lagrangian formulation to investigate the effect of coupling on resonant microstrip transmission line

Susanta Kumar Samanta[1], Rajib Pradhan[1] and Debapriyo Syam[2]

[1]Midnapore College, Midnapore 721101, India and [2]Guest Faculty, CAPSS, Bose Institute, Salt Lake, Kolkata 700091, India

Research Paper

Cite this article: Samanta SK, Pradhan R, Syam D (2023). Lagrangian formulation to investigate the effect of coupling on resonant microstrip transmission line. *International Journal of Microwave and Wireless Technologies* **15**, 298–310. https://doi.org/10.1017/S1759078722000277

Received: 6 August 2021
Revised: 3 February 2022
Accepted: 4 February 2022
First published online: 8 March 2022

Key words:
Filters; microstrip line; microwaves; resonance; sensors; split-ring resonator; terahertz

Author for correspondence:
Rajib Pradhan,
E-mail: rjbpradhan@yahoo.co.in

Abstract

An analytical and a numerical study on coupling in microstrip transmission line (MTL) are reported for different split-gap orientations of a single gap square-shaped split-ring resonator (SRR). Taking both magnetic and electric couplings and adopting Lagrangian formulation for this coupled system, mathematical relations are found for each orientation of SRR to determine the connection between coupling co-efficient and resonant mode frequency. It is shown that coupling results in higher resonance frequency when the SRR, with parallel split-gap, has the gap far from the MTL. But, a lower resonance frequency is obtained when the SRR is placed at shorter distances with parallel split-gap near to the MTL. Again, for perpendicular split-gap orientation of SRR, the resonant frequency is found in terms of an effective coupling co-efficient; at shorter distances it is found to be lower than the fundamental resonance frequency of uncoupled SRR and an opposite effect is obtained at longer distances. Using CST Microwave Studio, the resonance frequency for each split-gap orientation of SRR is also studied as a function of separation between MTL and SRR. It is observed that this phenomenon strongly depends on SRR side-length, substrate height, and separation between MTL and SRR.

Introduction

Metamaterials (MMs), also called left-handed materials, have simultaneously negative electrical permittivity ε_{eff} and negative magnetic permeability μ_{eff}. The split-ring resonators (SRRs) are main components of MMs. In 1999, the first SRR was proposed by Pendry as a resonant magnetic particle designed for effective negative permeability ($\mu_{eff} < 0$) [1]. The effective negative permeability in a certain frequency range can be obtained using suitable SRR geometries [2, 3]. When a time-varying magnetic field (H) is applied parallel to the axes of the rings, current induced on the surface of the ring will depend on the resonant properties of the structure. It can produce an internal magnetic field that may either enhance or oppose the incident field. Permeability (μ_{eff}) can be positive below the resonant frequency and it becomes negative at higher frequencies. Again, the effective negative permittivity ($\varepsilon_{eff} < 0$) of complementary SRRs (C-SSRs) was proposed to design narrow band-stop filters [4–6]. A microstrip line is a compact transmission line which is used to transmit microwave signals. Both SRR and C-SSR are able to pass/stop signal propagation through a transmission line at the fundamental resonance mode. The SRRs are generally small resonant elements with high-quality factor at microwave frequency. Now, the SRR loaded microstrip line can also offer a high Q-factor that is very useful for both microwave and terahertz bio-sensing applications [7–10] and also, for thin-film sensing applications [11]. The band-stop filter is one of the most important microwave components to filter out or to reject the unwanted signals, but pass desired signals. So, the band-stop filter plays a key role in the wireless systems. For stop-band response, the microstrip lines loaded with single SRR and also with cascaded SRRs for different orientations have been proposed in [7–13]. To calculate the resonance frequency of this type of coupled system, the equivalent circuit model may help us. The resonance frequency of this system will depend on electric and magnetic coupling coefficients which depend on geometrical properties of SRR and microstrip transmission line (MTL). Moreover, its resonance frequency will depend on the split-gap orientation of SRR.

A classical Lagrangian approach can be used for better understanding of the physics of the propagation phenomena through MTL. Earlier, the resonance properties with radiation properties of a magnetic dimer (MD) [14, 15] were successfully described by a quasi-molecular hybridization model using Lagrangian approach. An MD consists of two single-gap split-ring resonators coupled through magnetic induction. It has potential application for optical devices. Also, the near-field coupling within SRR-MMs [16] has been analyzed using Lagrangian approach, taking into account both the relative orientation and the offset between

CAMBRIDGE UNIVERSITY PRESS

the centers of two neighboring resonators. Here, both the electric and magnetic interaction coefficients have been calculated. Again, the magnetic dipole coupling between inner and outer SRRs [17] can show a strong magnetic interaction. By introducing magnetic and electric interaction terms into the Lagrangian formalism, the electromagnetic coupling effect on the magnetic resonant frequency was investigated. Moreover, the Lagrangian and dissipation functions have been proposed in typical dispersive and absorptive MMs with finite losses [18]. Also, a one-dimensional magnetic plasmon (MP) propagating in a linear chain of single SRRs was proposed in [19], where the sub-wavelength size resonators interact mainly through exchange of conduction current, resulting in stronger coupling as compared to the corresponding magneto-inductive interaction. To better understand the interactions involved in the splitting of the MP resonance, a comprehensive semi-analytical theory based on the attenuated Lagrangian formalism has been developed. In addition, a Lagrangian model has been presented to investigate the chiral optical properties of stereo-MMs [20], where the phase retardation effect due to the three-dimensional stacked configuration has been taken into consideration.

However, making use of the Lagrangian formulation, nobody has so far investigated the characteristics of a microstrip line coupled to a SRR. Here, a simple formula is derived to obtain the resonant mode frequency of this coupled system for three different configurations of SRR with transmission line. In loaded microstrip line, the coupling between electric dipoles together with coupling between magnetic dipoles may significantly affect the resonance characteristics. At resonance mode frequencies, the electromagnetic wave strongly couples with the SRR and produces an oscillating current in the structure. As a result, a strong electric field would be created in the split-gap. Also, a magnetic field cuts through the ring. In this work, the mutual inductance between MTL and SRR, and the changes in the capacitances of the MTL and the SRR due to the effects of coupling between MTL capacitance and SRR capacitance for parallel and perpendicular split-gap orientations of SRR have been analyzed for various separation distances between MTL and SRR, various side-lengths of SRR, and also, for various heights of the dielectric substrate. The magnetic coupling co-efficient between MTL and SRR, and also, the electric coupling co-efficient between MTL capacitance and SRR capacitance have been calculated for the various separation distances. The validity of the equivalent circuit models is confirmed by using CST Microwave Studio full-wave electromagnetic simulations. To model an SRR-loaded MTL with very high Q-factor, this type of analysis is very useful for microwave and terahertz bio-sensing, thin-film sensing, and also, for microwave filter applications.

Device description and Lagrangian formulation

A schematic diagram of a square-shaped SRR is shown in Fig. 1(a) and its equivalent circuit is presented in Fig. 1(b). An SRR consists of a magnetic loop with inductance L_S associated with the metal ring and a capacitance C_S that corresponds to the split-gap of the ring. (Actually, the side surface of the SRR also contributes to the capacitance.) Therefore, the SRR can be described as an equivalent L-C circuit with a fundamental resonance frequency of $\omega_0 = (L_S C_S)^{-\frac{1}{2}}$. Considering charge accumulation in the split-gap, the Lagrangian description of an SRR can be formulated in terms of the time-dependent charge (q) as the generalized coordinate and current ($\dot{q}$) as the corresponding velocity.

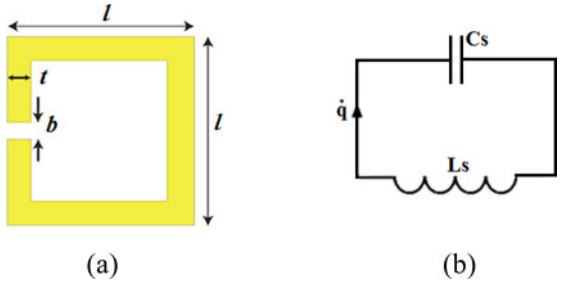

Fig. 1. (a) Schematic view of an uncoupled SRR, and (b) its equivalent circuit model.

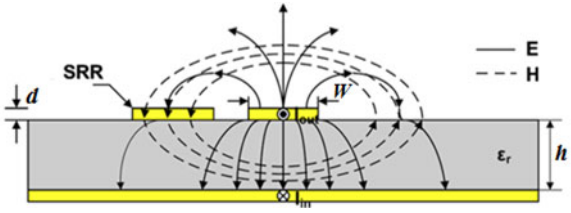

Fig. 2. Electric (E) and magnetic field (H) distribution associated with the microstrip line.

When the SRR is excited by an incident electro-magnetic wave, the Lagrangian can be written as [17]

$$\Im = \frac{1}{2} L_S \dot{q}^2 - \frac{1}{2} \frac{q^2}{C_S}, \tag{1}$$

where $\frac{1}{2} L_S \dot{q}^2$ and $\frac{1}{2} \frac{q^2}{C_S}$ refer to the kinetic energy stored in the loop and the electrostatic energy stored in the split-gap, respectively. So, the equation of motion (i.e. the Euler–Lagrange equation) is

$$\frac{d}{dt}\left(\frac{\partial \Im}{\partial \dot{q}}\right) - \frac{\partial \Im}{\partial q} = 0. \tag{2}$$

By solving Euler–Lagrange equation, it is straightforward to obtain the resonance frequency of SRR from

$$L_S \ddot{q} + \frac{q}{C_S} = 0 \tag{3}$$

or,

$$f_0 = \frac{1}{2\pi\sqrt{L_S C_S}}. \tag{4}$$

In calculating the resonance frequency of the SRR, its loss and radiation resistances are not considered in this circuit model.

A "SRR loaded microstrip line" is shown in Fig. 2. Taking its equivalent π-network model, the lumped parameters per section of the unloaded line comprise of an inductance (L) and a capacitance (C). In this circuit model, the losses are disregarded, which is a reasonable assumption for low-loss dielectric substrates. When the SRR is placed near to a microstrip line and they are excited, energy is exchanged between them through overlapping of their electric and magnetic fields. As a result, the system acts as a pair of coupled harmonic oscillators. Depending upon the relative orientation of SRR with respect to the MTL, the coupling via electric and magnetic dipole moments and higher moments

https://doi.org/10.1017/S1759078722000277 Published online by Cambridge University Press

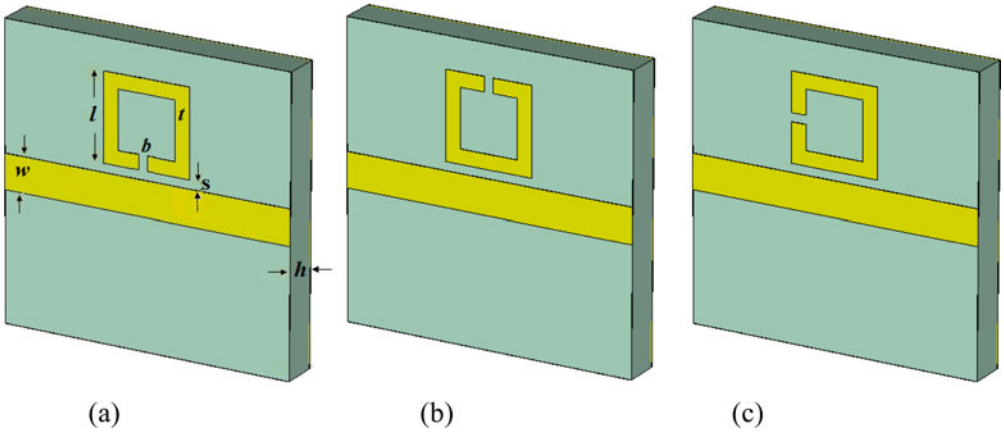

Fig. 3. Layout of SRR coupled microstrip line for (a) a parallel split-gap orientation near to the line, (b) a parallel split-gap orientation far from the line, and (c) a perpendicular split-gap orientation.

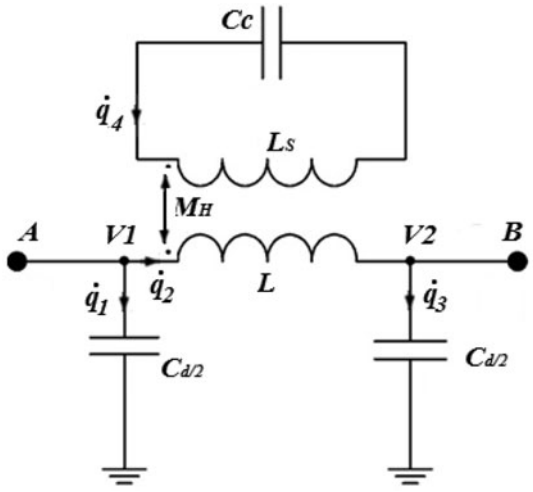

Fig. 4. Equivalent circuit model of coupled SRR and microstrip line is shown.

will vary. We shall analyze the nature of the couplings for various orientations of SRR by adopting the Lagrangian formalism. Figure 3 shows the layouts for three different split-gap orientation of SRR with MTL. The loaded SRR having parallel split-gap are of two types: (i) parallel split-gap of SRR near to the line in Fig. 3(a), and (ii) parallel split-gap of SRR far from the line in Fig. 3(b). Another has the split-gap of the SRR in perpendicular orientation, which is shown in Fig. 3(c).

With parallel split-gap orientation of SRR

Resorting to single-mode approximation, a lumped-element equivalent circuit (as in Ref. [13]) in Fig. 4 is considered to calculate the resonant mode frequency of this coupled system.

The Lagrangian formalism for this case runs as follows:

In view of the high Q-value ($\geq$10) of the device, and so, a small rate of energy dissipation and radiation in the microwave range, the kinetic energy term including magnetic interaction of the oscillators can be written as (using Refs [15–17])

$$T_M = \frac{1}{2}L\dot{q}_2^2 + \frac{1}{2}L_S\dot{q}_4^2 + M_H\dot{q}_2\dot{q}_4, \tag{5}$$

where the first two terms are energy stored in the inductors and the last term, having M_H, the mutual inductance, represents the energy associated with magnetic interaction. This quantity, M_H, can be positive or negative.

Again, the potential energy of this coupled system is

$$V_E = \frac{1}{2}\frac{q_1^2}{\frac{C_d}{2}} + \frac{1}{2}\frac{q_3^2}{\frac{C_d}{2}} + \frac{1}{2}\frac{q_4^2}{C_c} - V_1(q_1 + q_2) + V_2(q_2 - q_3), \tag{6}$$

where C_c and C_d are, respectively, the effective capacitance of the coupled SRR and microstrip line. The capacitance of a charged conductor increases if a metal sheet or strip is brought near it. This happens on account of the lowering of the potential of the charged conductor due to the induced charges of opposite sign on the strip. We may write $C_c = C_S + C_{SRR-MS}$; the change (C_{SRR-MS}) is roughly proportional to the inverse cube of the distance between SRR and MTL, and may also involve higher inverse-powers. A similar expression can be written for C_d. Basically, the distance between the two conductors is the distance between the split-gap and the microstrip line. The mutual inductance between the SRR and the MTL, on the other hand, varies inversely as (and also, the next few higher inverse-powers of) the distance between them since the magnetic field over the ring, due to the current in the MTL, varies roughly in that manner. Variation of resonance frequency can be explained on the basis of the natures of variation of C_{SRR-MS} and M_H.

Now, the Lagrangian for the system can be written as

$$\Im_E = \frac{1}{2}L\dot{q}_2^2 + \frac{1}{2}L_S\dot{q}_4^2 + M_H\dot{q}_2\dot{q}_4 - \frac{1}{2}\frac{q_1^2}{\frac{C_d}{2}} - \frac{1}{2}\frac{q_3^2}{\frac{C_d}{2}} - \frac{1}{2}\frac{q_4^2}{C_c} + V_1q_1 + V_2q_3 + q_2(V_1 - V_2). \tag{7}$$

The Euler–Lagrange equations of this coupled system are

$$\frac{d}{dt}\left(\frac{\partial\Im_E}{\partial\dot{q}_i}\right) - \frac{\partial\Im_E}{\partial q_i} = 0 \ (\text{where } i = 1,\ 2,\ 3,\ 4). \tag{8}$$

From (7) and (8), we obtain

$$q_1 = \frac{C_d V_1}{2}, \tag{9}$$

https://doi.org/10.1017/S1759078722000277 Published online by Cambridge University Press

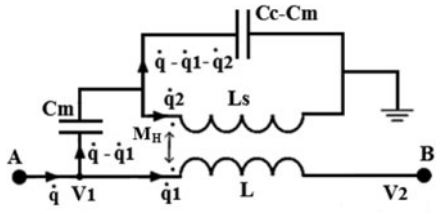

Fig. 5. Equivalent circuit model, for a loaded microstrip line with vertical split-gap SRR, is shown.

$$L\ddot{q}_2 + M_H\ddot{q}_4 - (V_1 - V_2) = 0, \tag{10}$$

$$q_3 = \frac{C_d V_2}{2}, \tag{11}$$

and

$$L_S\ddot{q}_4 + M_H\ddot{q}_2 + \frac{q_4}{C_c} = 0. \tag{12}$$

From (10) and (12), we get

$$L_S\ddot{q}_4 + M_H\left(\frac{-M_H\ddot{q}_4}{L}\right) + \frac{q_4}{C_c} + \frac{M_H}{L}(V_1 - V_2) = 0. \tag{13}$$

From (13), it is observed that when $V_1 = V_2$ (suggesting band pass filtering action) the SRR loaded microstrip line can be described by an oscillatory equation for the charge q_4:

$$\ddot{q}_4 + \frac{q_4}{C_c\left(L_S - \frac{M_H^2}{L}\right)} = 0. \tag{14}$$

So, the resonance mode frequency is

$$f_{\parallel} = \frac{1}{2\pi\sqrt{L_S C_c(1 - k_m^2)}}. \tag{15}$$

Here, $k_m\left(= M_H/\sqrt{LL_S}\right)$ is the magnetic coupling co-efficient between microstrip line and SRR.

Note that when the distance between the split-gap and the microstrip is small, the variation of C_{SRR-MS} with distance (rapid rise with decreasing distance) plays the dominating role in deciding how the resonance frequency changes. However, when the distance is large, the variation of M_H determines how resonance frequency changes.

With perpendicular split-gap orientation of SRR

An equivalent circuit (as in Ref. [13]), for the configuration having the split-gap of the SRR in perpendicular orientation with respect to the MTL, is shown in Fig. 5. The perpendicular component of the electric field of the MTL is parallel to the split-gap which causes a strong electric coupling. In the equivalent circuit model, C_m (called coupling capacitance) comes from this additional electric coupling between the microstrip line and the SRR.

Now, to calculate the resonance frequency, we again consider the Lagrangian formalism. Assuming no dissipation of energy as for the parallel split-gap orientation of SRR, the kinetic energy (using Refs [15–17]) is

$$T_M = \frac{1}{2}L\dot{q}_1^2 + \frac{1}{2}L_S\dot{q}_2^2 + M_H\dot{q}_1\dot{q}_2. \tag{16}$$

Also, the electrostatic energy is

$$V_E = \frac{1}{2}\frac{(q-q_1)^2}{C_m} + \frac{1}{2}\frac{(q-q_1-q_2)^2}{C_c - C_m} - (V_1 - V_2)q_1 - V_1(q-q_1). \tag{17}$$

Combining (16) and (17), and using the Euler–Lagrange formalism, the equations of motion are found to be

$$L\ddot{q}_1 + M_H\ddot{q}_2 - \frac{q-q_1}{C_m} - \frac{q-q_1-q_2}{C_c - C_m} + V_2 = 0, \tag{18}$$

$$L_S\ddot{q}_2 + M_H\ddot{q}_1 - \frac{(q-q_1-q_2)}{(C_c - C_m)} = 0, \tag{19}$$

and

$$\frac{(q-q_1)}{C_m} + \frac{(q-q_1-q_2)}{C_c - C_m} - V_1 = 0. \tag{20}$$

The condition for the resonance can be expressed as having nontrivial solutions for q and q_2 when the output voltage at port B, $V_2 = 0$ (i.e. $q_1 = 0$ at all times; hence, $\dot{q}_1 = \ddot{q}_1 = 0$.) So, our equations reduce to

$$M_H\ddot{q}_2 - \frac{q}{C_m} - \frac{q-q_2}{C_c - C_m} = 0, \tag{21}$$

$$L_S\ddot{q}_2 - \frac{(q-q_2)}{(C_c - C_m)} = 0, \tag{22}$$

and

$$\frac{q}{C_m} + \frac{(q-q_2)}{C_c - C_m} - V_1 = 0. \tag{23}$$

From (23), we have

$$\frac{(q-q_2)}{C_c - C_m} = \frac{C_m}{C_c}.\left(V_1 - \frac{q_2}{C_m}\right). \tag{24}$$

Moreover, using (23) in (21) we get

$$M_H\ddot{q}_2 = V_1. \tag{25}$$

Again, using (25), (23), and (24), we get

$$\left(L_S - \frac{C_m}{C_c}.M_H\right)\ddot{q}_2 + \frac{q_2}{C_c} = 0. \tag{26}$$

https://doi.org/10.1017/S1759078722000277 Published online by Cambridge University Press

This leads to the resonance mode frequency of the coupled system

$$f_{\perp} = \frac{1}{2\pi\sqrt{L_S C_c - C_m M_H}} = \frac{f_0}{\sqrt{1 + \frac{(L_S C_{SRR-MS} - C_m M_H)}{L_S C_S}}}. \quad (27)$$

The magnitude of $\frac{(L_S C_{SRR-MS} - C_m M_H)}{L_S C_S}$ is the square of the effective coupling co-efficient of this coupled system, and (27) can be re-written as

$$f_{\perp} = \frac{f_0}{\sqrt{(1 \pm k_E^2)}}. \quad (28)$$

In (28), the positive sign applies when $L_S C_{SRR-MS} > C_m M_H$ and the negative sign applies when $L_S C_{SRR-MS} < C_m M_H$. The quantity k_E is the effective coupling co-efficient between the microstrip line and the SRR for perpendicular split-gap orientation of SRR. So, the microstrip line may show a lower frequency resonance mode depending on the sign of C_m when coupled with an SRR with perpendicular split-gap. As $V_2 = 0$, this is the band stop or notch configuration. Note that there will be no effect on the resonance frequency if, for the perpendicular orientation of the gap, the split-gap appears in the opposite arm of the ring.

Simulation, calculation, and analysis: also comparison of analytical results with previously published results

To analyze the coupling between the microstrip line and the SRR for each split-gap orientation of SRR, the coupled mode frequency was computed for different separation distances between the nearest edges of the SRR and MTL. The variation of the coupled mode frequency was actually found for two alternative cases.

Variation with substrate height for a particular side-length of a square loop (we have taken l = 3 mm)

At first, we show in Fig. 6, the resonance mode frequencies as obtained for different coupling distances, which is the separation (denoted by s) between the nearest edges of an SRR and MTL, for the substrate height (h) of 0.65 and 1.27 mm. Also, the fundamental simulated resonance frequency of uncoupled SRR is shown for both cases in the mentioned figures.

It is observed that when the split-gap of the SRR is on the distant parallel arm, the coupled system shows a higher frequency resonance mode which decreases with the increase of separation. But, the resonance mode frequency increases with the increase in separation distance when the split-gap of the SRR is on the nearer parallel arm and also, with the perpendicularly oriented split-gap of SRR. Again, for the last two split-gap orientations, a lower frequency resonance mode occurs at shorter distances and the higher frequency resonance mode is obtained at larger separations. Due to a decrease of mutual inductance, beyond a certain distance, the mode frequencies settle down to the fundamental resonance frequency of uncoupled SRR at the substrate height of 1.27 mm (see Fig. 6(b)). But, for the decreased substrate height of 0.65 mm, the resonance mode frequency for SRR, with parallel split-gap near to the line and also for SRR with perpendicularly-oriented split-gap, increases above the fundamental resonance frequency of uncoupled SRR (i.e. 6.288 GHz) with an increase of separation from 0.3 to 0.7 mm as shown in Fig. 6(a). This happens due to the fact that the coupling capacitance (i.e. C_m) becomes negative (the current through it has reversed direction) and its magnitude increases after a certain separation gap between the MTL and the SRR. The variations of coupled mode frequency, as noted above, are consistent with theoretical expectations as outlined at the end of sub-section "Variation with substrate height for a particular side-length of a square loop (we have taken l = 3 mm)".

Now to calculate the value of mutual inductance (M_H) between MTL and SRR for various distances, we may use (15) for parallel split-gap far from the line. At first, the value of C_{SRR-MS} is assumed to be negligible with respect to C_S. Then, the resonance

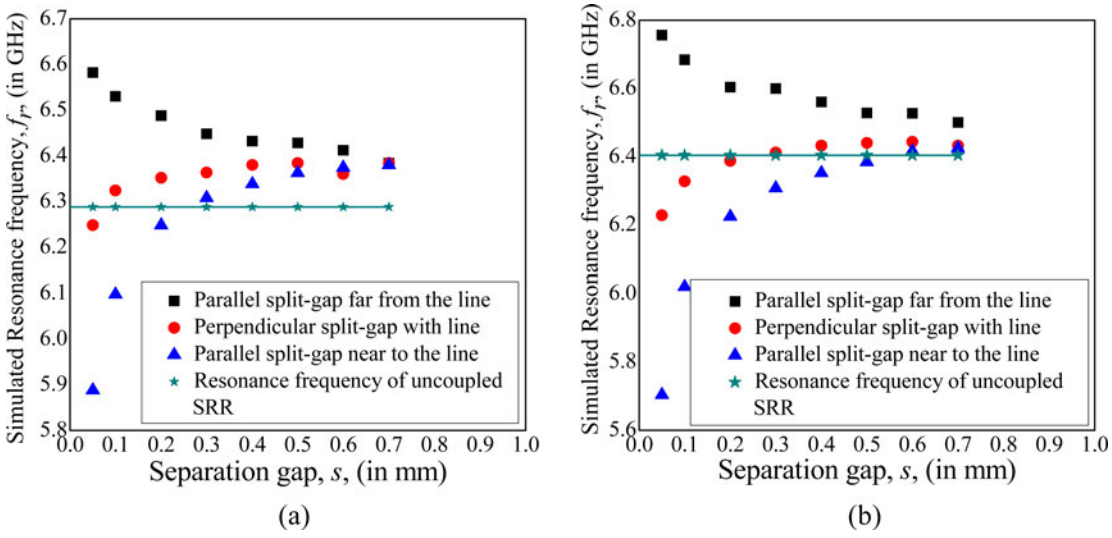

Fig. 6. Variations of resonance mode frequency with edge-to-edge separation between MTL and SRR, at a substrate height of (a) 0.65 mm, and (b) 1.27 mm, are shown for near, far, and vertical split-gap orientation of SRR.

https://doi.org/10.1017/S1759078722000277 Published online by Cambridge University Press

frequency of this coupled system can be written as

$$f_{\parallel\_f} \approx \frac{1}{2\pi\sqrt{L_S C_S(1-k_m^2)}} \approx \frac{f_0}{\sqrt{\left(1-\frac{M_H^2}{LL_S}\right)}}, \tag{29}$$

where L is the inductance of the uncoupled MTL. The inductance of an MTL can be written as [21]

$$L = \frac{60 l_1}{v}\ln\left[\frac{8h}{W}+\frac{W}{4h}\right] \text{for } \frac{W}{h} \le 1 \tag{30}$$

or,

$$L = \frac{120\pi l_1}{v}\left[\frac{1}{\frac{W}{h}+1.393+0.667\ln\left(\frac{W}{h}+1.444\right)}\right] \text{for } \frac{W}{h} > 1, \tag{31}$$

where l_1 and W are the length and width of the MTL, respectively. Also, v is the free space light velocity. Again, the self-inductance of a single gap square-shaped SRR can be written as [22]

$$L_S = \frac{2\mu_0}{\pi}\left[\ln(l) - \ln(t) + \left\{\sqrt{2}+2\ln 2 - \ln\left(\sqrt{2}+1\right) - 2\right\}\right] l, \tag{32}$$

where l and t are the side-length and width of the SRR, respectively. Further the capacitance of the single gap square-shaped SRR may be written as [22]

$$C_S = \frac{\varepsilon_0\varepsilon_g d.t}{b} + \varepsilon_0\varepsilon_g(d+b+t) + 2(d+t)\varepsilon_s C_{surf}^{pul}, \tag{33}$$

where d and b are the thickness and split-gap of the SRR. Also, ε_g is the effective dielectric constant of the substrate (on which the SRR is fabricated) for the capacitance associated with the split-gap and ε_s is the corresponding quantity for the capacitance associated with the side-surface of the ring.

To determine the analytical expression of C_S, the height of the dielectric substrate was considered to be infinite; in reality, this height is finite. Also, the effect of the metal sheet (on which the substrate is deposited) has not been considered for finding L_S and C_S. So, to rectify the error (i.e. in order to find the actual uncoupled resonance frequency from the analytical value), it is necessary to calibrate an SRR against simulated resonance frequency, for different substrate heights. For three different sides length of SRR (keeping fixed the other geometrical parameters), the calibration factor (=ratio of simulated SRR resonance frequency to analytical SRR resonance frequency) is plotted in Fig. 7 for various substrate heights. It is observed that for the side-length of 3 mm and the substrate height of 1.27 mm, the simulated SRR resonance frequency is close to analytical SRR resonance frequency.

Now, using simulation data for $f_{\parallel\_f}$ and f_0, and putting the analytical values of L and L_S, we can evaluate the apparent

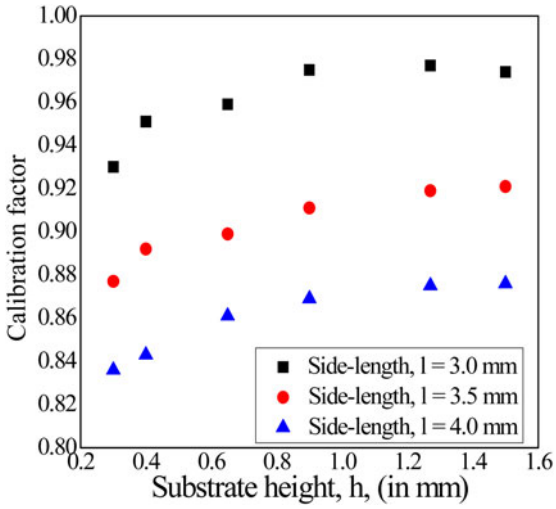

Fig. 7. Variation of calibration factor with substrate height is shown for three different values of side-length keeping fixed the other geometrical parameters of the coupled system.

value of M_H for different intermediate distances (i.e. the distance of mid-point of the loop from the line which is assumed to be $d_2 = (s + l/2)$, where l is the side-length of SRR loop). Plotting M_H versus $(s + l/2)$ graph and fitting the nature of M_H by $b_1/d_2 + b_2/d_2^2 + b_3/d_2^3 + b_4/d_2^4$, the coefficients b_1, b_2, b_3, and b_4 could be determined. After that, putting the value of M_H, the values of C_{SRR-MS} at different separation gaps (i.e. where $d_1 = (s + t/2)$, t is the width of the SRR), could be calculated from resonance frequency data for SRR with near parallel split-gap, given by

$$f_{\parallel\_n} = \frac{f_0}{\sqrt{\left(1+\frac{C_{SRR-MS}}{C_S}\right)\left(1-\frac{M_H^2}{LL_S}\right)}}. \tag{34}$$

Next, plotting C_{SRR-MS} versus $(s + t/2)$ for near parallel split-gap orientation, and fitting the nature of C_{SRR-MS} by $a_1/d_1^3 + a_2/d_1^4$, we can work out approximate values of the two constants a_1 and a_2. Now, the contribution of C_{SRR-MS} may be considered in (15) for parallel split-gap far from the line, when the separation gap is to be considered as $d_3 = (s + l - t/2)$. After that, a revised value of M_H could be determined from (34) and thereafter the constants b_1, b_2, b_3, and b_4 could be found properly from the plot of M_H versus $(s + l/2)$. Also, plotting k_m versus $(s + l/2)$ graph and fitting the nature of k_m by $c_1/d_2 + c_2/d_2^2 + c_3/d_2^3 + c_4/d_2^4$, the coefficients c_1, c_2, c_3, and c_4 could be determined. Once more, a plot of C_{SRR-MS} versus $(s + t/2)$ would have to be made and fitting the data for C_{SRR-MS}, we can determine improved values of the constants a_1 and a_2.

At first, for the substrate height of 0.65 mm, we have calculated the values of M_H, k_m, and C_{SRR-MS} at various distances from MTL and plotted these in Figs 8(a)–8(c), respectively. Moreover, considering the analytical values of C_S and C_{SRR-MS} at vertical split-gap with different separation gaps, and using (27), the C_m may be calculated for different distances. Also, the value of electric coupling co-efficient (k_e) between C and C_S can be calculated for different separation gaps.

https://doi.org/10.1017/S1759078722000277 Published online by Cambridge University Press

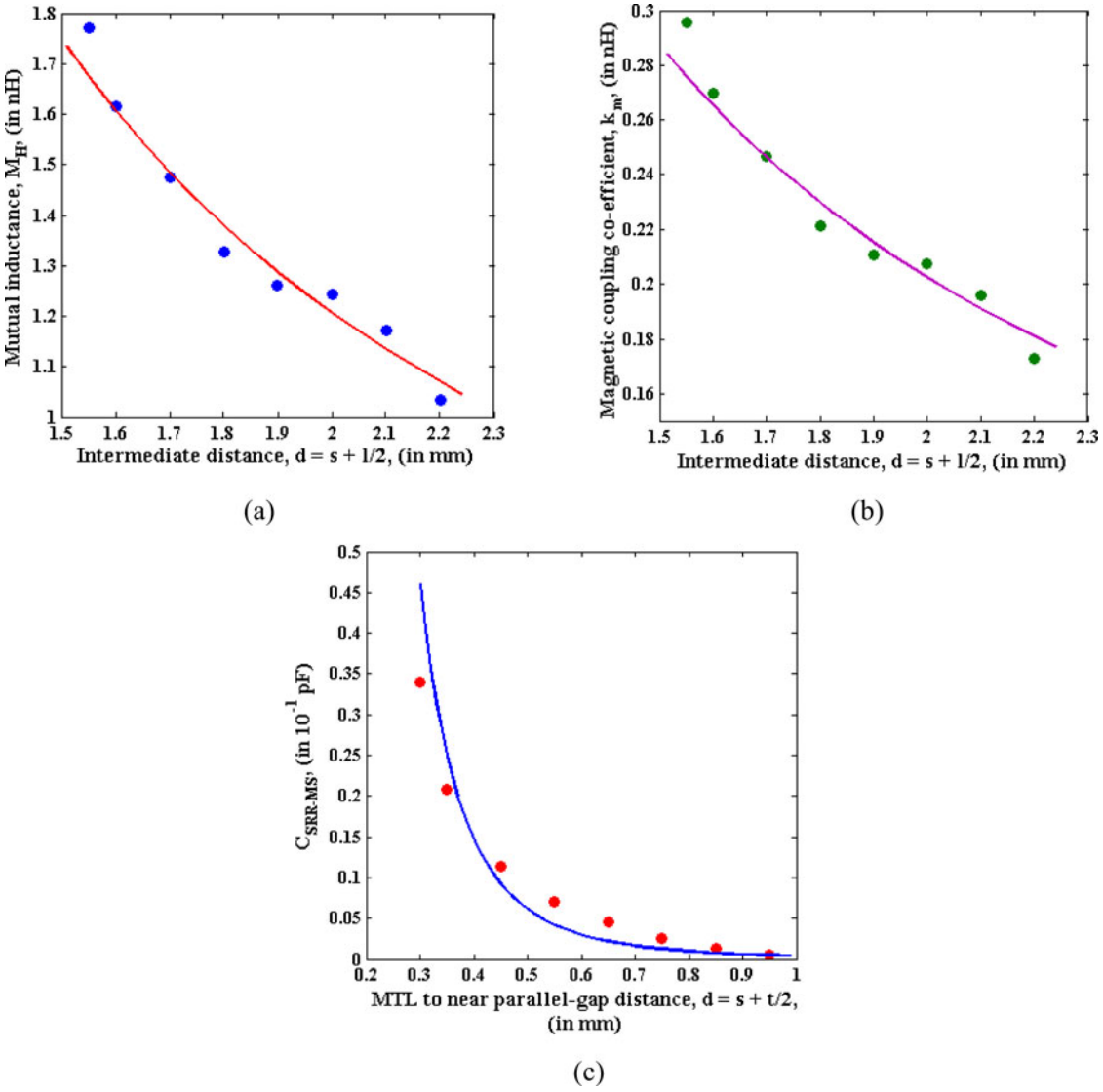

Fig. 8. Variations with distance of (a) mutual inductance, (b) magnetic coupling coefficient, and (c) the change in SRR capacitance are plotted for SRR at a side-length of 3 mm and a substrate height (h) of 0.65 mm.

The MTL capacitance per unit length (C_1) may be written as [23]

$$C_1 = \frac{0.67(1.41 + \varepsilon_r)}{\ln\left\{\frac{5.98h}{0.8W + d}\right\}}, \tag{35}$$

where d is the thickness of the MTL which is identical to the thickness of the SRR. Also, ε_r is the dielectric constant of the substrate.

A list of analytical and simulated parameters is given in Table 1 for the substrate heights of 0.65 and 1.27 mm.

Similar calculations have also been made for the substrate height of 1.27 mm and the corresponding plots are shown in Figs 9(a)–9(c). With perpendicular orientation of SRR split-gap, the mode frequency of the coupled MTL is above the uncoupled SRR resonance frequency for edge-to-edge separation between MTL and SRR of 0.05–0.7 mm. The list of calculated values of constants from Figs 9(a)–9(c) is given in Table 2 for two different substrate heights.

Table 1. List of parameters to draw Figs 8 and 9

Substrate height (h) (in mm)	Simulated SRR resonance frequency (f_0) (in GHz)	L_S (in nH)	C_S (in pF)	L (in nH)	C (in pF)
0.65	6.288	4.100	0.1430	8.749	5.189
1.27	6.404	4.106	0.1436	8.660	5.242

https://doi.org/10.1017/S1759078722000277 Published online by Cambridge University Press

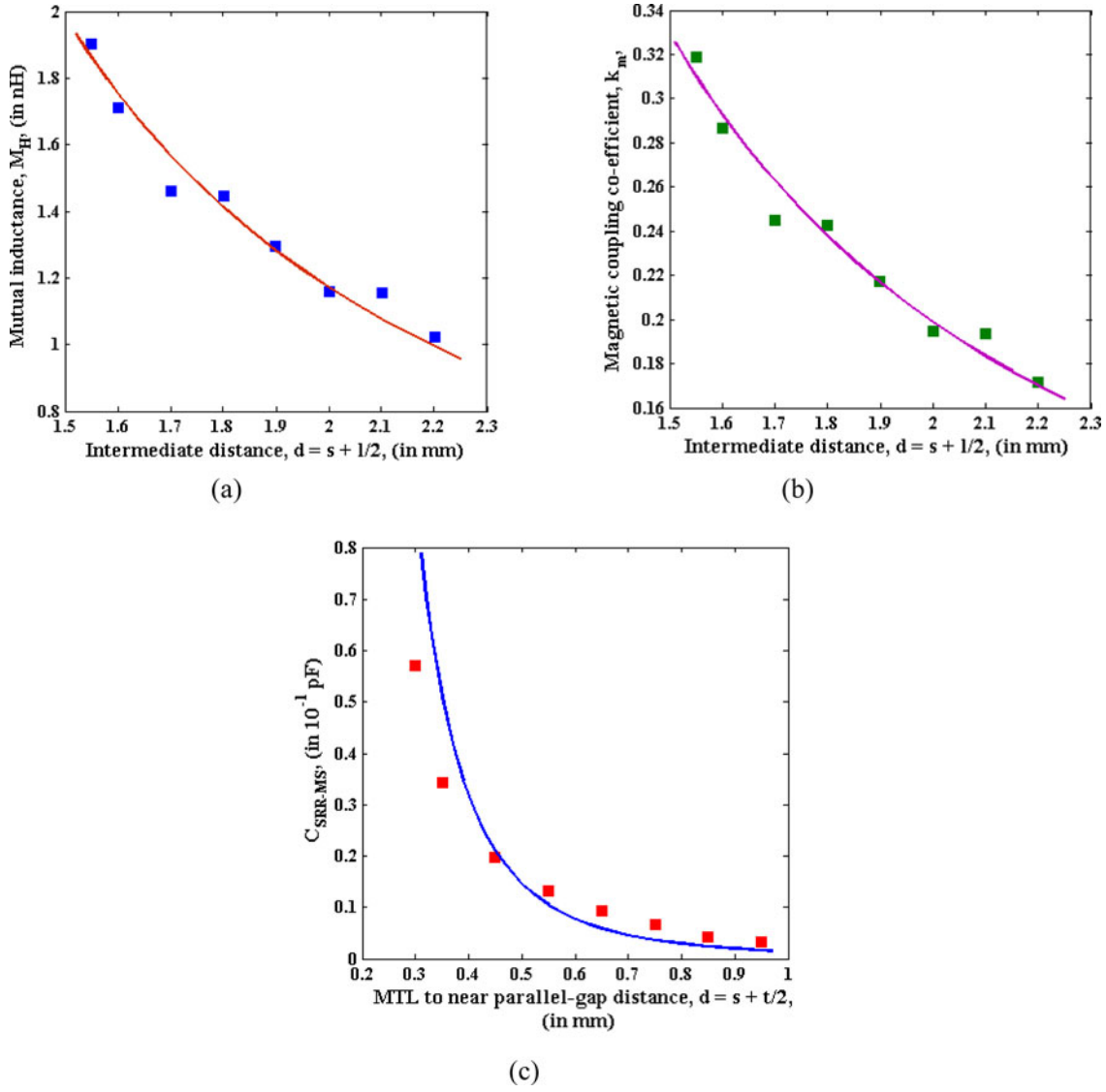

Fig. 9. For MTL ,with SRR having a side-length of 3 mm and a dielectric substrate height of 1.27 mm, the (a) mutual inductance, (b) magnetic coupling co-efficient, and (c) the change in SRR capacitance.

Table 2. List of fitted constants for a split-ring with a side-length of 3 mm and the substrate heights of 0.65 and 1.27 mm

Substrate height (h) (in mm)	b_1 (in nH-m)	b_2 (in nH-m^2)	b_3 (in nH-m^3)	b_4 (in nH-m^4)
0.65	1.80×10^{-3}	1.19×10^{-6}	0.07×10^{-9}	–
1.27	1.07×10^{-3}	1.61×10^{-6}	1.87×10^{-9}	
	c_1 (m)	c_2 (in m^2)	c_3 (in m^3)	c_4 (in m^4)
0.65	0.34×10^{-3}	0.11×10^{-6}	0.04×10^{-9}	–
1.27	0.21×10^{-3}	0.22×10^{-6}	0.31×10^{-9}	
	a_1 (in pF m^3)	a_2 (in pF m^4)		
0.65	0.43×10^{-13}	0.36×10^{-15}		
1.27	9.61×10^{-13}	0.43×10^{-15}		

*Variation with side-length of a square loop for a particular substrate height (*h *= 1.27 mm)*

In this sub-section, Figs 10(a) and 10(b) are drawn to display the effect of coupling for different separations (i.e. s) between the nearest edges of the SRR and MTL for a particular substrate height of 1.27 mm, and SRR side-lengths of 3.5 and 4.0 mm. It is observed that the uncoupled resonance frequency of SRR decreases with an increase of side-length and also, the resonance mode frequency of MTL decreases at different separation distances.

https://doi.org/10.1017/S1759078722000277 Published online by Cambridge University Press

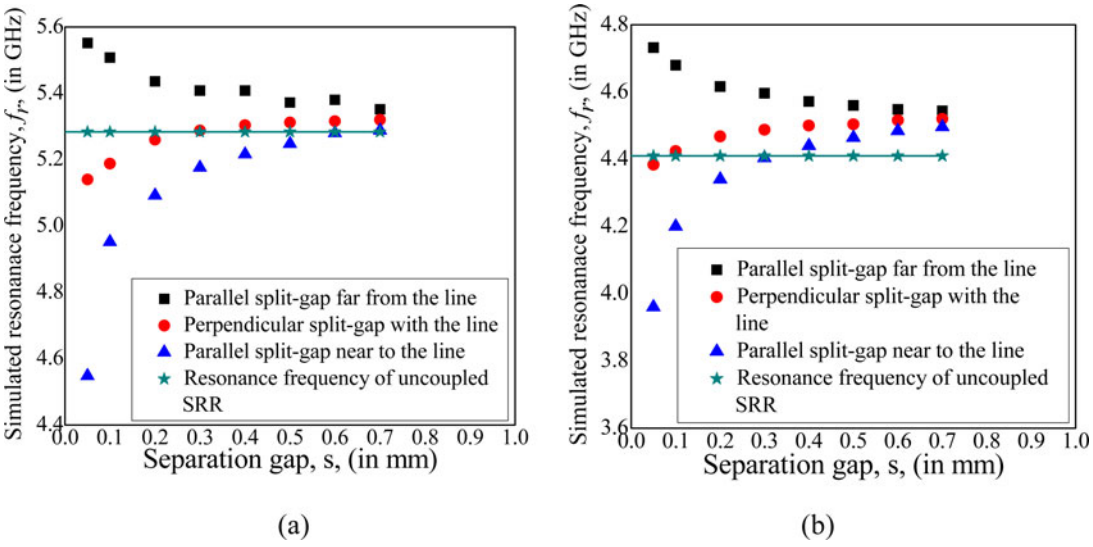

Fig. 10. Variations of resonance mode frequency of MTL, with separation from SRR, are shown for near, far, and vertical split-gap configurations, for SRRs with a side-length of 3.5 mm (Fig. 10(a)) and 4 mm (Fig. 10(b)) when substrate height is 1.27 mm.

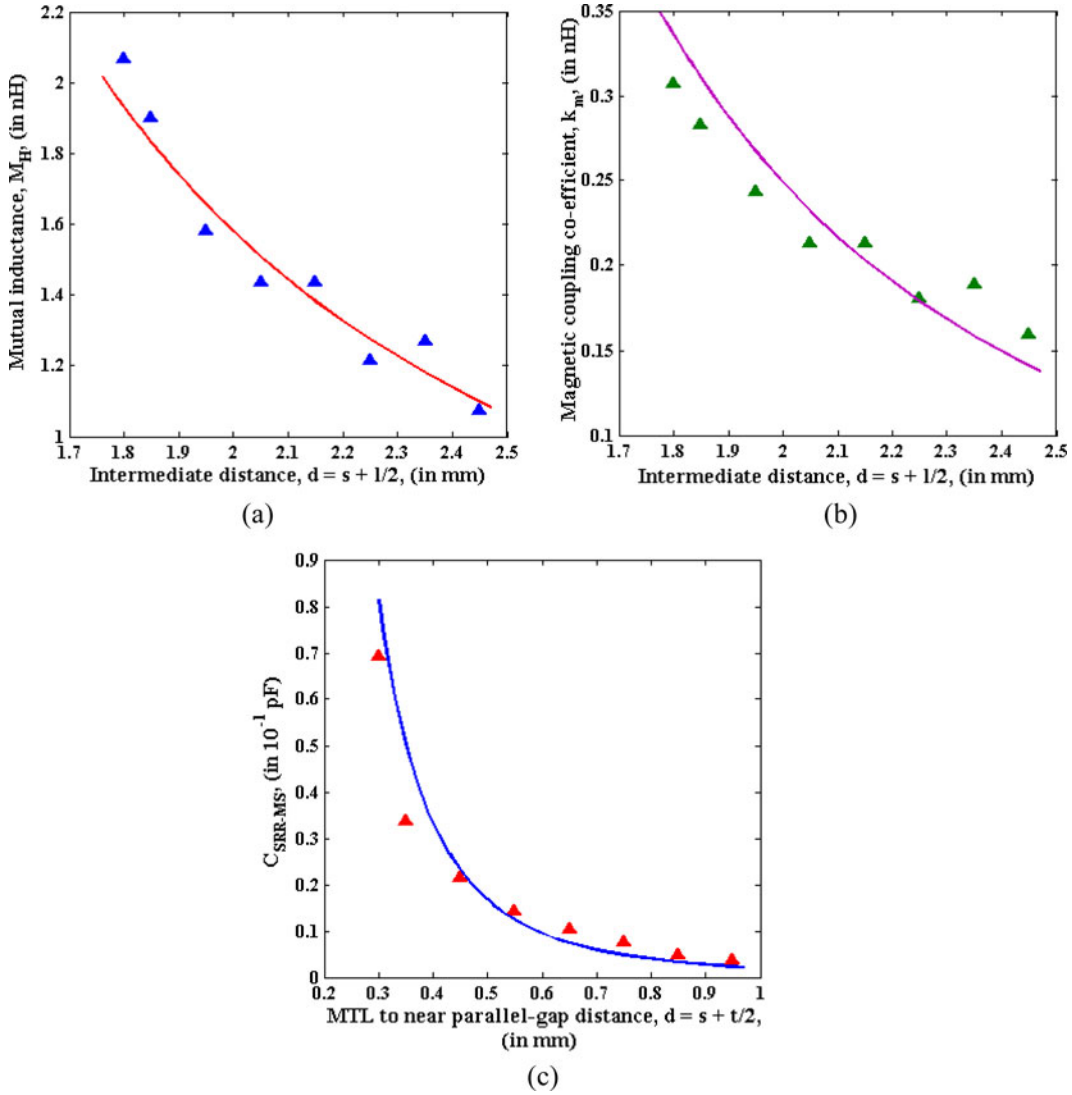

Fig. 11. Variations, with separation distance, of (a) mutual inductance, (b) magnetic coupling co-efficient, and (c) C_{SRR-MS}, are plotted for MTL with SRR having a side-length of 3.5 mm and a substrate height (h) of 1.27 mm.

https://doi.org/10.1017/S1759078722000277 Published online by Cambridge University Press

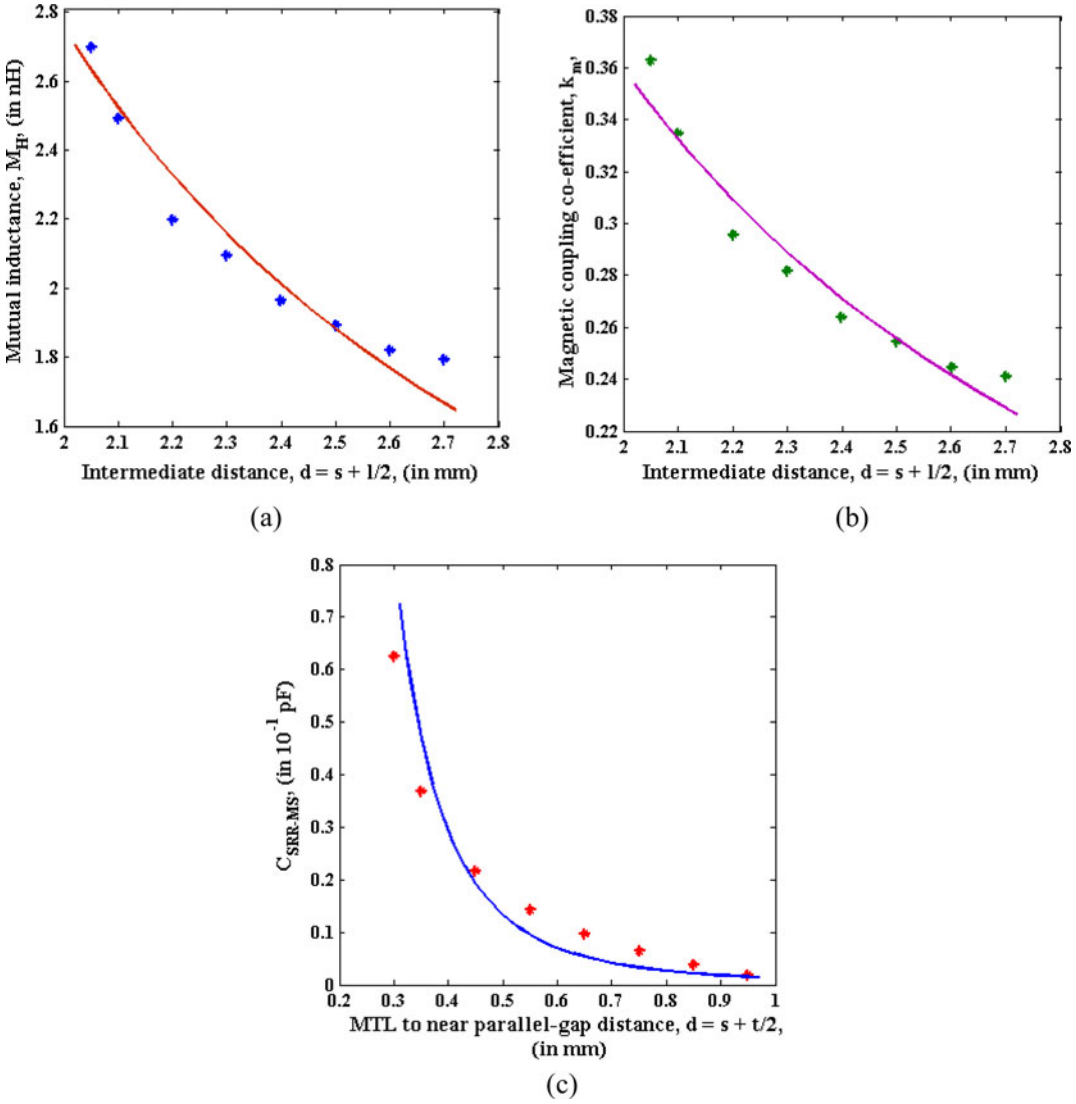

Fig. 12. Plots of (a) mutual inductance, (b) magnetic coupling co-efficient, and (c) C_{SRR-MS} are shown for different separation distances for MTL with SRR having a side-length of 4 mm and a substrate height (h) of 1.27 mm.

For the SRR with a side-length of 3.5 mm, numerical calculations have been carried out to study the variations of different parameters such as M_H, k_m, and C_{SRR-MS} as shown in Figs 11(a)–11(c), as functions of separation distances. The results of similar calculations for the SRR of side-length of 4 mm are shown in Figs 12(a)–12(c).

In Table 3 are shown the fitted constants for the SRR having a side-length of 3.5 and 4 mm, respectively. Other analytical and

Table 3. List of fitted constants for a side-length of 3.5 and 4 mm for a substrate height of 1.27 mm

Side-length (l) (in mm)	b_1 (in nH-m)	b_2 (in nH-m^2)	b_3 (in nH-m^3)	b_4 (in nH-m^4)
3.5	1.41×10^{-3}	1.52×10^{-6}	3.95×10^{-9}	–
4.0	2.81×10^{-3}	2.87×10^{-6}	3.15×10^{-9}	3.77×10^{-12}
	c_1 (m)	c_2 (in m^2)	c_3 (in m^3)	c_4 (in m^4)
3.5	0.03×10^{-3}	0.05×10^{-6}	1.77×10^{-9}	–
4.0	0.47×10^{-3}	0.19×10^{-6}	0.43×10^{-9}	0.37×10^{-12}
	a_1 (in pF m^3)	a_2 (in pF m^4)		
3.5	19.01×10^{-13}	0.09×10^{-15}		
4.0	8.35×10^{-13}	0.41×10^{-15}		

https://doi.org/10.1017/S1759078722000277 Published online by Cambridge University Press

Table 4. List of parameters to draw Figs 11 and 12

Side-length of SRR (l) (in mm)	Simulated SRR resonance frequency (f_0) (in GHz)	L_S (in nH) (in nH)	C_S (in pF)	L (in nH)	C (in pF)
3.5	5.284	5.222	0.1469	8.661	5.242
4.0	4.410	6.390	0.1498	8.660	5.242

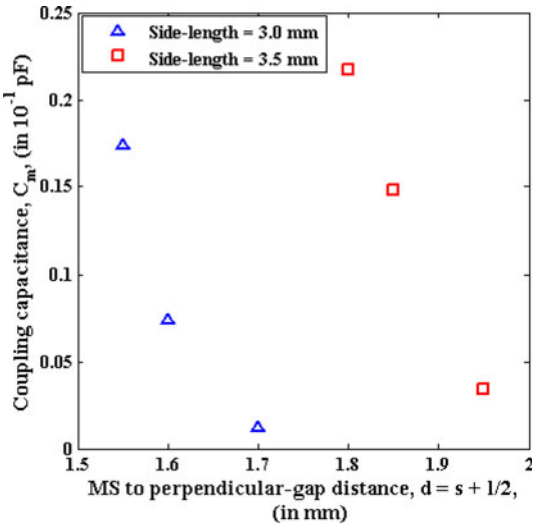

Fig. 13. The coupling capacitance is plotted for different separation distances between MTL and SRR, with SRR having a side-length of 3 and 3.5 mm.

simulation parameters are presented in Table 4 for this coupled system for a substrate height of 1.27 mm. Again, the calculated value of C_m has been shown for different distances in Fig. 13 (substrate height = 1.27 mm) for a side-length of 3.0 and 3.5 mm. It is observed that the coupling capacitance decreases with distance and it shows larger value for SRR of a side-length of 3.5 mm. The C_m is not considered at higher edge-to-edge separation between MTL and SRR due to un-physical (negative) result in C_m value. For a side-length of 4 mm, C_m is positive over a very small range of SRR to MTL distance. This is the reason why we have no data corresponding to a side-length of 4 mm in Fig. 13.

We can also calculate the electric coupling coefficient (k_e) between C and C_S at perpendicular split-gap orientation of SRR with respect to the MTL.

For our calculations, the analytical values of L_S and C_S are considered. But, the simulated resonance frequency of uncoupled SRR is used to calculate M_H, k_m, C_{SRR-MS}, and C_m. The analytical resonance frequencies are 6.557, 5.748, and 5.145 GHz for SRR side-length of 3, 3.5, and 4 mm, respectively, which differ from the simulated values, i.e. 6.404, 5.284, and 4.410 GHz, respectively.

Table 5. List of geometrical parameters of the coupled system

Symbols	Parameters	Dimension (in mm)
W	Width of the microstrip line	1.2
h	Thickness of the dielectric substrate	0.65 and 1.27
d	Thickness of the SRR	0.017
l	Arm length of the SRR	3, 3.5, and 4
t	Width of the SRR	0.5
b	Split-gap in the SRR	0.3
l_1	Length of the MTL	20

The list of other geometrical parameters which were used in simulations appears in Table 5. In our FW simulation, the Rogers (RO3010) has been assumed to be the substrate with a dielectric constant $\varepsilon_r = 10.2$.

To compare with analytical results in [13], our analytical formula has been used to determine magnetic coupling co-efficient (i.e. k_m) and electric coupling co-efficient (i.e. k_e) for the given geometrical parameters in that reference. It is observed that our analytical value for k_m and k_e match well with the analytical results in that reference. The variation may be attributed to the difference in simulated resonance frequencies due to the use of different software. These are shown with the geometrical parameters in Table 6. The magnetic coupling coefficient between MTL and SRR, and the coupling capacitance between MTL capacitance and SRR capacitance for perpendicular split-gap orientation are shown in Table 6. In that table, the geometrical parameter values shown are the same as in Ref. [13]. In [13], the MTL inductance and capacitance, and also, the SRR inductance and

Table 6. List of geometrical parameters of the coupled system in [13] and comparison between analytical results

Parameters value	According to reference [13]	Our results
Width of the microstrip line = 1.2 mm	Magnetic coupling co-efficient = 0.28	0.31
Microstrip line and SRR thickness = 0.017 mm		
Side-length of SRR = 3.0 mm		
Width of the SRR = 0.2 mm	Coupling capacitance = 0.055 (pF)	0.067 (pF)
Split-gap of the SRR = 0.5 mm		
Separation between SRR and microstrip line = 0.1 mm		
Substrate dielectric constant = 10.2		

https://doi.org/10.1017/S1759078722000277 Published online by Cambridge University Press

Table 7. List of *Q*-factors with variation of side-length for different split-gap orientation.

For side-length	With near parallel split-gap of SRR	With far parallel split-gap of SRR	With perpendicular split-gap of SRR
3.0 mm	114	22	25
3.5 mm	101	21	21
4.0 mm	88	20	21

capacitance have been found under coupled condition for a particular separation distance. The line parameters (i.e. L, C) have been obtained using LINPAR software under coupled condition. Then, the magnetic coupling co-efficient has been calculated using closed-form expressions for the resonance frequency and the minimum reflection frequency. To calculate the coupling capacitance, and also to find both sets of coupling coefficients at different coupling distances, it was necessary to repeat the analysis process. But, in our method, we do not need to repeat the analysis. Just putting the separation distance in the fitting formula and using appropriate coefficient values, we can find the coupling capacitance and the coupling coefficients.

Using our parameters, we have calculated the *Q*-factor of this coupled system taking 1.27 mm as the substrate height and the edge-to-edge separation between SRR and MTL of 0.1 mm which is given in Table 7. The *Q*-factor is defined as $f_0/\Delta f$, where Δf is the bandwidth at −3 dB and also, f_0 is the center frequency. It is seen that the *Q*-factors are almost similar (about 22) for parallel split-gap of SRR far from the line and perpendicular split-gap SRR. But, for parallel split-gap of SRR near to the line, it is very high (about 100).

Conclusion

We have adopted the classical Lagrangian approach to determine the resonance mode frequency of an MTL for different split-gap orientations of a coupled single gap square-shaped SRR. For various separation distances (between the MTL and the SRR), the coupled resonance frequency of microstrip line has also been determined with a commercial full-wave electromagnetic time-domain solver, CST Microwave Studio, based on the Finite-Integration Technique (FIT) for three different configurations of the split-gap. It has been observed that the MTL, with SRR having parallel split-gap far from the line, shows a coupled resonant mode with a higher frequency; but MTL with SRR having parallel split-gap near to the line has a lower frequency resonance mode at shorter separation distances and a higher frequency resonance mode at larger separation distances with respect to the fundamental resonance frequency of uncoupled SRR. Also, the system displays both of these features when the split-gap of the SRR is set perpendicularly to the MTL. Again, with the increase of substrate height from 0.65 to 1.27 mm, keeping fixed the other geometrical parameters, the simulated resonance frequency of uncoupled SRR was found to increase to a higher value and the lower frequency resonance mode started at larger distances as shown in Fig. 6. On the other hand, the opposite phenomena occur with an increase of side-length of the square loop as shown in Fig. 10. Using the expressions for resonance mode frequency, the mutual inductance between MTL and SRR, the magnetic coupling co-efficient between MTL and SRR, the change in SRR capacitance due to close placement of two conductors (i.e. MTL and SRR) and also, the coupling capacitance between MTL and SRR for perpendicular split-gap orientation have been studied for different separation distances with changing substrate height and side-length of the SRR in Figs 8, 9, 11–13, respectively. It is observed that the mutual inductances as shown in Figs 8(a), 9(a), 11(a), and 12(a), the change in SRR capacitances as shown in Figs 8(c), 9(c), 11(c), and 12(c), and the coupling capacitances as shown in Fig. 13 decrease with the separation distance. The results of calculations for the magnetic coupling co-efficient are shown for different separation distances in Figs 8(b), 9(b), 11(b), and 12(b), respectively. The fit parameters are presented in Tables 2 and 3. In addition, the list of analytical and simulated parameters is given in Tables 1 and 4. Also, a list of the geometrical parameters for this coupled system is given in Table 5. From our calculations, the simulated values of uncoupled SRR resonance frequency are 6.404, 5.284, and 4.410 GHz, respectively, for SRR side-length of 3, 3.5, and 4 mm. But the analytical resonance frequencies are 6.557, 5.748, and 5.145 GHz, respectively, for SRR side-length of 3, 3.5, and 4 mm, which are somewhat different from the simulated values. It is due to the assumption of infinite height of dielectric substrate; also, the effect of the metal sheet (on which the substrate is deposited) has not been considered for finding L_S and C_S. So, to rectify the error (i.e. in order to find the actual uncoupled resonance frequency from the analytical value), SRRs have been calibrated against substrate height for three different SRR side-lengths (keeping fixed the others geometrical parameters) by comparison with simulated resonance frequency, as shown in Fig. 7. It is observed that the simulated SRR resonance frequency decreases with an increase of SRR side-length. Also, the SRR shows higher resonance frequency for larger values of the substrate height. In our analysis, the magnetic coupling coefficient has been assumed (quite reasonably) to have the same value for all split-gap orientations at a particular edge-to-edge separation between MTL and SRR. Additionally, to justify our analytical model, a comparison has been made between our analytical results and the analytical results in Ref. [13]. This type of coupled system with very high *Q*-factor under particular coupling conditions is required to design notch filter and various bio-sensors in microwave and terahertz regimes.

Acknowledgements. Rajib Pradhan is grateful to the Research Centre of Midnapore College, India.

Financial support. Scheme of RUSA 2.0 component: 8 (620/MC/RUSA-2.0/PROJECT/19/13(7)).

Conflict of interest. None.

References

1. **Pendry JB, Holden AJ, Robins DJ and Stewart WJ** (1999) Magnetism from conductors and enhanced non-linear phenomena. *IEEE Transactions on Microwave Theory and Techniques* **47**, 2075–2084.
2. **Smith DR, Padilla WJ, Wier DC, Nemat-Nasser SC and Schultz S** (2000) Composite medium with simultaneously negative permeability and permittivity. *Physical Review Letters* **84**, 4184–4187.
3. **Marques R, Mesa F, Martel J and Medina F** (2003) Comparative analysis of edge- and broad side coupled split ring resonators for metamaterial design-theory and experiments. *IET Microwaves, Antennas & Propagation* **51**, 2572–2581.
4. **Katsarakis N, Koschny T, Kafesaki M, Economou EN and Soukoulis CM** (2004) Electric coupling to the magnetic resonance of split ring resonators. *Applied Physics Letters* **84**, 2943–2945.

https://doi.org/10.1017/S1759078722000277 Published online by Cambridge University Press

5. **Falcone F, Lopetegi T, Baena JD, Marqués R, Martín F and Sorolla M** (2004) Effective negative-ε stop band microstrip lines based on complementary split ring resonators. *IEEE Microwave and Wireless Components Letters* **14**, 280–282.
6. **Bonache J, Gil M, Gil I, García-García J and Martín F** (2006) On the electrical characteristics of complementary metamaterial resonators. *IEEE Microwave and Wireless Components Letters* **16**, 543–545.
7. **Asci C, Sadeqi A, Wang W, Nejad HR and Sonkusale S** (2020) Design and implementation of magnetically-tunable quad-band filter utilizing split-ring resonators at microwave frequencies. *Scientific Reports* **10**, 1–4.
8. **Taher Al-Nuaimi MK and Whittow WG** (2010) Compact microstrip band stop filter using SRR and CSSR: design, simulation and results. Proceedings of the Fourth European Conference on Antennas and Propagation 2010.
9. **Hu X, Zhang Q and He S** (2009) Dual-band-rejection filter based on split ring resonator (SRR) and complimentary SRR. *Microwave and Optical Technology Letters* **51**, 2519–2522.
10. **Cinar A and Bicer S** (2020) Band-stop filter design based on split ring resonators loaded on the microstrip transmission line for GSM-900 and 2.4 GHz ISM band. *International Advanced Researches and Engineering Journal* **04**, 029–033.
11. **Chen T, Li S and Sun H** (2012) Metamaterials application in sensing. *Sensors* **12**, 2742–2765.
12. **Kshetrimayum RS, Kallapudi S and Karthikeyan SS** (2008) Stop band characteristics for periodic patterns of CSRRs in the ground plane and its applications in harmonic suppression of band pass filters. *International Journal of Microwave and Optical Technology* **3**, 88–95.
13. **Bojanic R, Milosevic V, Jokanovic B, Medina-Mena F and Mesa F** (2014) Enhanced modelling of split-ring resonators couplings in printed circuits. *IEEE Transactions on Microwave Theory and Techniques* **62**, 1605–1615.
14. **Liu H, Genov DA, Wu DM, Liu YM, Liu ZW, Sun C, Zhu SN and Zhang X** (2007) Magnetic plasmon hybridization and optical activity at optical frequencies in metallic nanostructures. *Physical Review B* **76**, 073101-1–073101-4.
15. **Li TQ, Liu H, Li T, Wang SM, Cao JX, Zhu ZH, Dong ZG, Zhu SN and Zhang X** (2009) Suppression of radiation loss by hybridization effect in two coupled split-ring resonators. *Physical Review B* **80**, 1151131–1151136.
16. **Powell DA, Lapine M, Gorkunov MV, Shadrivov IV and Kivshar YS** (2010) Metamaterial tuning by manipulation of near-field interaction. *Physical Review B* **82**, 155128-1–155128-8.
17. **Jing F, Guang-Yong S and Wei-Ren Z** (2011) Electric and magnetic dipole couplings in split ring resonator metamaterials. *Chinese Physics B* **20**, 114101–114106.
18. **Pi-Gang Luan J** (2018) Lagrangian dynamics approach for the derivation of the energy densities of electromagnetic fields in some typical metamaterials with dispersion and loss. *Physical Communication* **2**, 075016–075017.
19. **Liu H, Genov DA, Wu DM, Liu YM, Steele JM, Sun C, Zhu SN and Zhang X** (2006) Magnetic plasmon propagation along a chain of connected subwavelength resonators at infrared frequencies. *Physical Review Letters* **97**, 249302–249304.
20. **Liu H, Cao JX and Zhu SN** (2010) Lagrange model for the chiral optical properties of stereometamaterials. *Physical Review B* **81**, 241403–241404.
21. **Paul CR** (2010) *Inductance: Loop and Partial*, 2nd Edn. Hoboken, NJ, Canada: John Wiley & Sons, Inc.
22. **Samanta SK, Pradhan R and Syam D** (2021) Theoretical approach to verify the resonance frequency of a square split ring resonator. *Journal of the Optical Society of America B: Optical Physics* **38**, 2887–2897.
23. **Paul CR** (2008) *Analysis of Multiconductor Transmission Lines*, 2nd Edn. Hoboken, NJ, Canada: John Wiley & Sons, Inc., pp. 144–147.

Susanta Kumar Samanta received his B.Sc. degree in physics from the Vidyasagar University, Midnapore, India in 2011. He has also received his M.Sc. degree in electronics from the same university in 2013. He is currently working toward the Ph.D. degree. His main area of research interest is electromagnetic metamaterials.

Rajib Pradhan received his Ph.D. degree on modeling of vertical cavity semiconductor saturable absorber for all-optical device applications from Vidyasagar University, West Bengal, India in 2018. He joined the Department of Physics Midnapore College, India in 2006 as an Assistant Professor. His present interest is (i) semiconductor optical amplifier and semiconductor saturable absorber-based photonic devices, (ii) dissipative soliton and cavity soliton, (iii) microwaves and terahertz metamaterials, and (iv) split-ring resonator-based transmission line for microwave device applications.

Debapriyo Syam was born on August 27, 1953. He was educated in Kolkata (Calcutta). He received the M.Sc. degree in physics from Calcutta University and the Ph.D. degree in high energy physics from the Saha Institute of Nuclear Physics affiliated to Calcutta University. He taught at various Government Colleges of West Bengal, including the Presidency College (renamed Presidency University). From mid-1990s, he worked on theoretical and experimental aspects of nuclear track detectors, as well as on theoretical astroparticle physics, with collaborators from the Bose Institute (Calcutta). From September 2013 to August 2021, he was associated with the Centre for Astroparticle Physics and Space Science (CAPSS) at the Bose Institute. Apart from hard-core research he is interested in writing articles for students and teachers of undergraduate colleges.

https://doi.org/10.1017/S1759078722000277 Published online by Cambridge University Press